The role of the mean state on MJO simulation in CESM2 ensemble simulation

Daehyun Kang[1], Daehyun Kim[1], Min-Seop Ahn[1], Richard Neale[2], Jiwoo Lee[3], and Peter Glecker[4]

[1]University of Washington
[2]National Center for Atmospheric Research (UCAR)
[3]Lawrence Livermore National Laboratory, California, USA
[4]LLNL

November 21, 2022

Abstract

This study examines the role of the mean state in the propagation of the Madden-Julian Oscillation (MJO) over the Maritime Continent (MC). We use an ensemble of simulations made with a single model - the Community Earth System Model version 2 (CESM2) – to assess the effect of the mean state that is unaffected by that of model components such as parameterization schemes. Results show that one ensemble member with an exceptionally stronger MJO propagation also exhibits a much steeper background meridional moisture gradient (MMG) over the southern MC region than the other ensemble members. The simulated mean state affects MJO via its impacts on moisture dynamics - a column water vapor budget reveals a greater advection of mean moisture by MJO wind in the southern MC is responsible for the anomalous MJO activity.

The role of the mean state on MJO simulation in CESM2 ensemble simulation

Daehyun Kang[1], Daehyun Kim[1*], Min-Seop Ahn[2], Richard Neale[3], Jiwoo Lee[2], and Peter J. Gleckler[2]

[1]*Department of Atmospheric Sciences, University of Washington, Seattle, WA*

[2]*Lawrence Livermore National Laboratory, Livermore, CA*

[3]*National Center for Atmospheric Research, Boulder, CO*

to be submitted to the Geophysical Research Letters

July 2020

*Corresponding author: Daehyun Kim (daehyun@uw.edu)

Key Points

1. One member in a 10-member CESM2 ensemble simulation shows exceptionally pronounced MJO propagation over the Maritime Continent (MC).

2. The ensemble member with enhanced MJO propagation exhibits a steeper background moisture gradient around MC than the other members.

3. The steeper background meridional moisture gradient strengthens moisture recharging to the east of MJO, leading its eastward propagation.

Abstract

This study examines the role of the mean state in the propagation of the Madden-Julian Oscillation (MJO) over the Maritime Continent (MC). We use an ensemble of simulations made with a single model - the Community Earth System Model version 2 (CESM2) – to assess the effect of the mean state that is unaffected by that of model components such as parameterization schemes. Results show that one ensemble member with an exceptionally stronger MJO propagation also exhibits a much steeper background meridional moisture gradient (MMG) over the southern MC region than the other ensemble members. The simulated mean state affects MJO via its impacts on moisture dynamics - a column water vapor budget reveals a greater advection of mean moisture by MJO wind in the southern MC is responsible for the anomalous MJO activity.

Plain Language Summary

The MJO is planetary-scale, eastward moving envelope of anomalous convection. It is a dominant mode of dynamically coupled sub-seasonal variability in the tropics. Unfortunately, an accurate representation of the MJO has historically been a challenging task for many, if not most, global climate models. The mean state distribution of atmospheric moisture has been highlighted as a key aspect affecting the simulation of MJO propagation in many recent modeling studies. When many different models are compared, however, it is difficult to isolate the role of the mean state because different models use different parameterizations of moist physics that affect both the mean state and the MJO directly. In this study, we examine the relationship between the mean state and MJO propagation in an ensemble of simulations made with a single coupled model – CESM2. Each ensemble member differs only in its initial conditions and thus the parameterizations and resolution are identical. MJO propagation over the MC in the ten ensemble members of CESM2 is strongly affected by the background MMG, which is independent of the effect of moist physics. The background MMG is affected by ENSO-like internal variability that is tightly coupled with sea surface temperature over the Indo-Pacific warm pool.

1. Introduction

The Madden–Julian Oscillation (MJO, Madden & Julian 1971, 1972), the dominant mode of tropical intraseasonal variability, is an eastward propagating, planetary-scale envelop of anomalous convection coupled with circulation anomalies throughout the troposphere. The convection and circulation anomalies associated with the MJO exert substantial impacts on various weather and climate phenomena (Zhang, 2013), and thereby the MJO provides a major source of predictability in the subseasonal-to-seasonal time scales (Jones et al., 2004; Neena et al., 2014). Unfortunately, however, an accurate representation of the MJO has historically been a challenging task for many, if not most, global climate models (Kim et al., 2009; Hung et al., 2013; Ahn et al., 2017).

Linear perturbation theory (Holton & Hakim, 2013) is a widely accepted framework to study the dynamics of wave-like fluid motions. The basic state around which the wave perturbations are defined is almost always a key aspect of the system determining the fluid wave motion characteristics such as phase speed and growth rate. Similarly, it has long been speculated that poor simulation of the MJO by General Circulation Models (GCMs) is due to the biases in the basic state (Slingo et al. 1996; Inness et al. 2001; Kim et al. 2009; Gonzalez & Jiang 2017; Jiang 2017; Ahn et al. 2020b). For example, Slingo et al. (1996) found that models with more realistic simulation of the climatological seasonal cycle tend to exhibit better intraseasonal variability.

There are at least two factors that make characterizing the role of the GCM basic state in the MJO particularly challenging. From a modeling point of view, the cumulus parameterization, which is known to have substantial impacts on simulated MJOs (see Kim & Maloney 2017 for a review), also affects the mean state (Kim et al. 2011; Mapes & Neale 2011; Ahn et al. 2019).

Because changes in the convection scheme can affect the MJO both *directly* by altering how convection interacts with its large-scale environment and *indirectly* via their impacts on the basic state, separating the latter from the former is a non-trivial task (e.g., Peatman et al. 2018). In a similar vein, the atmosphere-ocean feedback, which is also known as a crucial factor for realistic MJO simulation, affects not only the MJO-related surface flux anomalies but also the meridional gradient of mean state moisture around the equator (DeMott et al., 2019).

From a theoretical point of view, it has remained elusive as to which aspects of the basic state are key to an accurate simulation of the MJO. Reflecting on the lack of consensus, previous studies have emphasized, rather empirically, the distribution of mean precipitation (Slingo et al. 1996; Kim et al. 2009) and the westerly basic state wind near the equator (Inness et al. 2001). Kim et al. (2011), who suggested that the conventional ways of improving the MJO tended to degrade the mean state, examined pattern correlations between the simulated and observed seasonal mean rain rate distributions. Ling et al. (2017) suggested that GCMs with poor MJO performance (as gauged by conventional metrics) had infrequent MJO events, which occurs only when the mean state is occasionally supportive of the MJO. However, they did not specify the aspects of the basic state that set favorable conditions for MJO emergence.

Recently, guided by the moisture mode theory of the MJO (Raymond & Fuchs 2009; Sobel & Maloney 2012; 2013; Adames & Kim 2016), which explains the propagation and maintenance of the MJO by those of column-integrated moisture anomalies, many studies have suggested that the horizontal gradient of mean moisture around the Maritime Continent (MC) is the aspect of the mean state that is key to a skillful MJO simulation (Gonzalez & Jiang 2017; Jiang 2017; Ahn et al. 2020b). It was shown that models with a relatively good MJO simulation skill tend to have a more realistic background moisture distribution with a steeper horizontal moisture gradient in the vicinity of the MC region (Gonzalez & Jiang 2017). With the steeper moisture gradient, the good-MJO models better represent horizontal moisture advection (Jiang, 2017), the process responsible for MJO's eastward movement (Maloney 2009; Kiranmari & Maloney 2011; Kim et al. 2014; Sobel et al. 2014). Ahn et al. (2020b) showed that the models participating in the CMIP6 tend to better simulate MJO propagation over the MC than the CMIP5 models and attributed the improvement to those in the horizontal gradient of background moisture near the MC area.

While the above-mentioned model intercomparison studies have shown a statistically robust relationship between the mean state moisture gradient and the MJO, it remains unclear how much of the inter-model difference in MJO simulation fidelity is due to the difference in the mean state. Because the models included in the intercomparison studies differ in their parameterization schemes (notably the cumulus scheme), for example, it is difficult to isolate the effects of the mean state from those of the parameterization schemes. In this study, to assess the role of the background moisture gradient on MJO propagation that is independent of the effect of model physics and other model configurations such as horizontal resolution, we use a ten-member ensemble simulation made with a single model that simulates a reasonable MJO. Specifically, this study addresses the following two questions: i) Do the MJO characteristics differ substantially within the ensemble simulations of a single model? and, if so, ii) Can the intra-ensemble differences be explained by variations in the background moisture gradient? It will be shown that the eastward propagation of the MJO over the MC region is much more pronounced in one ensemble member, which, relative to the other nine realizations, has a noticeably stronger meridional gradient of mean moisture near the MC region.

This manuscript is organized as follows. Section 2 describes the data and methodology employed in our study. In Section 3, we examine an ensemble spread of MJO propagation for the last two decades (1995-2014) based on the moisture mode framework, then the basic state affecting the ensemble spread is identified. Section 4 presents the summary and conclusions.

2. Data and Method

2.1 Dataset

The primary dataset used in this study is the Coupled Model Intercomparison Project phase 6 (CMIP6; Eyring et al. 2016) Historical simulations made with the Community Earth System Model version 2 (CESM2; Danabasoglu et al., 2020). The Historical simulation covers the period from 1850-2014 and is driven by best estimates of historical anthropogenic emissions. CESM2 captures the observed characteristics of the eastward propagation of MJO realistically (e.g., Ahn et al. 2020b, also see Figure 1). We obtained ten ensemble members, which will be referred to E1-E10, that differ from each other only in their initial conditions. The Tropical Rainfall Measuring Mission 3B42 version 7 (TRMM 3B42v7; Huffman et al. 2007) precipitation product used for verifying MJO simulation fidelity for a recent 20-year period (1999-2018). Atmospheric field variables are obtained from the fifth generation of the European Centre for Medium-Range Weather Forecasts (ECMWF) reanalysis (ERA5; Hersbach et al. 2019). A sea surface temperature (SST) product is obtained from the Hadley Centre Sea Ice and Sea Surface Temperature (Rayner 2003). All analysis was performed after interpolating data onto a 2.5 longitude × 2.5 latitude horizontal grid and for boreal winter (November–April).

2.2 Methods

To diagnose MJO propagation characteristics, intraseasonal (20-100 days) precipitation anomalies near the equator (10^{o}S-10^{o}N) were regressed onto intraseasonal precipitation anomalies averaged over the equatorial Indian Ocean (IO; 85°E-95°E, 5°S-5°N) and plotted in a lag-longitude diagram (e.g., Figure 1). We have adopted the 'MC propagation metric' of Ahn et al. (2020b) that was designed to quantitatively assess the robustness of the MJO's eastward propagation over the MC. The metric is obtained by averaging positive regression coefficients in the lag-longitude diagram over lag days 0-25 and longitudes 100-150^{o}E (red box in Figure 1) and then normalizing the resulting value by the corresponding value from observations. Ahn et al. (2020b) demonstrated that the metric is useful in assessing GCM simulation fidelity of the MJO's propagation over the MC region. Note that the ensemble numbers (E1-E10) are designated by their MC propagation metric values so that the metric value increases with the assigned ensemble number (Figure 1b).

The column-integrated moisture budget of the MJO is analyzed following Adames (2017), who divided the budget terms by the convective moisture adjustment time scale ($\overline{\tau}_{\mathrm{c}}$):

$$\frac{1}{\overline{\tau}_{\mathrm{c}}}\frac{\partial\langle q\rangle'}{\partial t} = \frac{1}{\overline{\tau}_{\mathrm{c}}}\left\{-\left\langle u\frac{\partial q}{\partial x}\right\rangle' - \left\langle v\frac{\partial q}{\partial y}\right\rangle' + C'\right\};\tag{1a}$$

$$C' = -\left\langle \omega\frac{\partial q}{\partial p}\right\rangle' - P' + E',\tag{1b}$$

where q is specific humidity, and u, v, and ω are the zonal, meridional, and vertical pressure velocities, respectively. P and E are precipitation and evaporation, respectively. The angled brackets indicate a mass-weighted vertical integral from the surface to 100 hPa, and the prime symbol denotes intraseasonal (20–100 days) anomalies. C denotes the 'column process' (Chikira

2014), including the vertical advection of moisture, precipitation, and evaporation, which is obtained as a residual. $\overline{\tau_c}$ is obtained using the following equation:

$$\overline{\tau_c} = \frac{\langle \overline{q_s} \rangle}{a\overline{P}} \ , \tag{2}$$

where $\langle \overline{q_s} \rangle$ is column-integrated saturation specific humidity. Overbars in Eq. (2) indicate 100-day low-pass-filtered variables. The sensitivity parameter a was obtained from the non-linear fit between column relative humidity and precipitation using data from each ensemble member, then averaged across all members (=7.9). To examine the relative roles of the mean state and MJO circulation, the meridional moisture advection term in Eq. (1a) was decomposed as:

$$-\mathrm{v}\frac{\partial \mathrm{q}}{\partial \mathrm{y}} \cong -\bar{\mathrm{v}}\frac{\partial \bar{\mathrm{q}}}{\partial \mathrm{y}} - \bar{\mathrm{v}}\frac{\partial \mathrm{q}'}{\partial \mathrm{y}} - \bar{\mathrm{v}}\frac{\partial \mathrm{q}''}{\partial \mathrm{y}} - \mathrm{v}'\frac{\partial \bar{\mathrm{q}}}{\partial \mathrm{y}} - \mathrm{v}'\frac{\partial \mathrm{q}'}{\partial \mathrm{y}} - \mathrm{v}'\frac{\partial \mathrm{q}''}{\partial \mathrm{y}} - \mathrm{v}''\frac{\partial \bar{\mathrm{q}}}{\partial \mathrm{y}} - \mathrm{v}''\frac{\partial \mathrm{q}'}{\partial \mathrm{y}} - \mathrm{v}''\frac{\partial \mathrm{q}''}{\partial \mathrm{y}} \ , \tag{3}$$

where the overbar, prime, and double prime denote the 101-day running mean, 20–100 day band-pass filtered anomaly, and 20-day high-pass filtered anomaly, respectively. The budget results were not sensitive to the horizontal interpolation technique used (not shown).

3. Results

Figure 1 presents the characteristics of MJO propagation in observations and the CESM2 ensemble simulations. The observed MJO precipitation anomalies move eastward from the IO to the western Pacific across the MC (Figure 1a). The MC propagation metric values obtained from individual ensemble members (Figure 1b) exhibit a marked spread, ranging from 0.76 to 1.30, even though the identical model is used (see Figure S1 for the lag-longitude diagrams for individual members). Interestingly, E10 shows the MC propagation metric that is exceptionally (~60%) higher than the rest. The value for E10 is also about 30% greater than that for E9, which has the second-largest value of the metric. The spread among the 10-member ensemble indicates substantial internal variability exists in the simulated MJO variability from 20-year segments, a finding consistent with the Crueger et al. (2013) demonstration of a notable spread in the MJO skill metric within the ECHAM6 ensemble simulations. In the following, we will examine the extent to which the inter-ensemble spread in MJO characteristics among CESM2 simulations is due to the differences in the mean state. Specifically, we will focus on understanding the difference between E10 and the ensemble-mean of the other nine members (hereafter EM19).

The EM19 exhibits a realistic eastward propagation of the MJO-associated precipitation anomalies (Figure 1c), although the phase speed of the eastward propagation is somewhat too fast. E10 shows much stronger precipitation anomalies over the MC than EM19 (Figure 1d-e). The lag-longitude diagrams in Figure 1 also show anomalous moisture recharging (contours) before the peak of positive precipitation anomalies across the Indo-Pacific warm pool in both observations (Figure 1a) and the simulations (Figures 1c and 1d), indicating that the eastward propagation of MJO precipitation is coupled with that of moisture anomalies. Furthermore, Figure 1e shows that the greater MJO MC precipitation anomalies in E10 can be traced to the greater moisture recharging locally, with about ten days of lead time. It seems from Figure 1e that understanding the difference in moisture tendency at lag days -5 to 5 is the key to understand the abnormally strong MJO signature in the MC in E10.

Figure 2 shows boreal winter climatology in EM19 (contours) and difference between E10 and EM19 (shaded) for surface temperature, and precipitable water (PW) and its meridional gradient. EM19 reproduces the observed climatology realistically. In particular, the mean PW is meridionally confined near the equator to the west of the dateline (Figure 2b), which corresponds to the positive (negative) meridional moisture gradient (MMG) to the south (north) of the equator (Figure 2c). The surface temperature difference between E10 and EM19 presents a central-Pacific El Nino-like pattern, with significant warming in the western-central Pacific Ocean and the equatorial IO (Figure 2a). However, the pattern is slightly shifted to the west when compared to that of the observed central-Pacific El Nino events exhibiting warming near the dateline (e.g., Kug et al. 2009). E10 shows the highest and lowest occurrences of El Nino and La Nina events for 1995-2014 respectively (Figure S2), indicating that the mean state difference seen in Figure 2 is likely due to the imbalance in the number of El Nino and La Nina events in E10.

The pattern of the mean PW difference (Figure 2b) resembles that of surface temperature, showing a wetter condition to the east and west of the MC near the equator, and a dryer condition at the off-equatorial MC regions especially in the southern hemisphere. As a result, the background MMG becomes steeper across the MC within the equatorial latitude band (10°S-10°N), where the difference in MJO propagation appears (Figure 1e). Note that the difference in the background MMG shown in Figure 2 is not due to the difference in MJO activity, which remains unchanged when calculated without strong MJO days (Figures S3b and S4). If the mean state difference in MMG in the MC can cause the difference in the rate of moistening before the onset of precipitation anomalies there, it would strongly support the notion that the difference between E10 and EM19 in their MJO characteristics is due to the difference in the mean state MMG. It appears that the mean state biases over the Indo-Pacific warm pool are larger in E10 than EM19, indicating the mean state in E10 is not necessarily more realistic than that in EM19 (Figure S5).

Figure 3 compares horizontal patterns of precipitation (shaded) and moisture tendency (contours) anomalies at different lag days. On lag day -5, in both E10 and EM19, the MJO precipitation anomalies are centered around the eastern equatorial IO. As in observations, the "vanguard" precipitation anomalies (Peatman et al., 2014) develop in Borneo and New Guinea islands during this time, which is slightly stronger in E10 than in EM19. As the MJO convection approaches the MC islands, E10 shows stronger precipitation anomalies near the Sumatra-Java islands (100-120°E) than those in EM19 (lag days 0-5). On lag day 10, a noticeable difference in precipitation anomalies appears over the northeastern MC (NMC; 130-150°E, Eq.-10°N). The difference in precipitation anomalies is proceeded by the difference in moisture tendency, as in Figure 1e. In the SMC (100-150°E, 10°S-Eq.; red box in Figure 3c on lag day -5), enhanced moistening during lag days -5 to 0 leads to the stronger precipitation anomalies on lag 5. Likewise, in the NMC (red box in Figure 3c on lag day 5), the greater moisture tendency anomalies on lag day 5 results in more prominent precipitation anomalies on lag 10.

To further examine moisture recharging processes over the SMC and NMC regions, in Figure 4 we compare moisture budget terms in the two areas. The higher total moisture tendency over the SMC on lag day -5 in E10 can primarily be attributed to the meridional advection term (Figure 4a). Note that the values of the total moisture tendency and meridional advection terms in E10 are outside the range from all the other ensemble members. Zonal advection term is also relatively higher in E10 than that in EM19, while the column process partly cancels out the difference caused by the horizontal advection terms. The timescale decomposition of the meridional advection term (Eq. 3) indicates that the advection of the mean moisture by intraseasonal wind anomalies dominates the difference between E10 and EM19 (Figure 4b). That the advection of the mean moisture by MJO wind anomalies is the key process for MJO propagation suggests that the moisture recharging in the SMC is directly enhanced by the steeper background MMG. Many previous observational and modeling studies also emphasized the role of the mean state moisture gradient in that region (Kim et al., 2014; Jiang 2017; Demott et al. 2018; Ahn et al. 2020a). Supporting the argument above, the ten ensemble members show a robust correlation between the area-averaged MMG in the SMC (70°-160°E, 10°S-2.5°S; the box in Figure 2c) and the MC propagation metric (R=0.89; Figure S3a).

The total moisture tendency over the NMC on lag 5 is much larger in E10 than in the other ensemble members, which is also predominantly due to the meridional moisture advection term (Figure 4c). Note that some members even exhibit negative moisture tendency. Unlike in the SMC, however, the advection of the mean moisture by perturbation winds does not seem to be able to explain the higher meridional moisture advection over the NMC in E10. Instead, the high-frequency eddy terms and the advection of anomalous moisture by anomalous winds (sixth and third terms in Figure 4d) play the dominant role. These terms in the NMC are likely to be affected by the larger moisture recharging around the New Guinea during lag -5-0 (Figure 3c), which gives a steeper anomalous intraseasonal moisture gradient between the New Guinea and the NMC. The high-frequency eddy term, which represents the strength of mixing between relatively moist near-equator and relatively dry subtropical air masses by synoptic-scale eddies (Andersen & Kuang, 2012; Maloney, 2009), can also be larger with the steeper intraseasonal moisture gradient. Additionally, we note that the intraseasonal easterly anomalies in the NMC on lag 5 are stronger in E10 than in EM19, which could further enhance the high-frequency eddy mixing process. The synoptic-scale high-frequency eddy activity can be suppressed in the intraseasonal easterly anomalies, resulting in the anomalous moistening near the NMC by reducing dry meridional advection from the subtropics (Maloney, 2009). The bigger contribution from the terms that are related to anomalous moisture gradient indicates the difference in the moisture recharging in the NMC is a consequence of the MJO-associated anomalies in E10 being stronger there than those in EM19.

By contrasting E10 with EM19, we demonstrate that a steeper background MMG can lead to stronger MJO propagation across the MC by enhancing the MJO-related moisture recharging. In order to explore the extent to which the conclusion holds beyond one example (E10), we expanded our analysis into the entire period of the Historical simulations (1851-2014). The ensemble mean of the area-averaged MMG in the SMC (the box in Figure 2c) does not show either a linear trend or a noticeable variation (Figure S6), suggesting that the MMG variability is predominantly due to the internal variability. When two groups of five 20-year epochs with the highest and the lowest MMG are compared, their differences in the mean state and the MJO propagation are consistent with the differences between E10 and EM19 (Figures S7 and S8).

4. Summary and Conclusion

Motivated by the recent studies highlighting the role of mean state moisture in the simulation of the MJO, we have examined the basic state and MJO propagation in a ten-member ensemble simulation made with a single model, the CESM2. Unlike the previous analysis of multi-model ensemble (Gonzalez & Jiang, 2017; Jiang, 2017; Ahn et al. 2020b), in which the separation of the role of the mean state from that of the model physics is difficult, our assessment is unaffected by differences in the parameterization scheme.

We found that one ensemble member (E10) showed MJO propagation over the MC that was much more pronounced than in the other ensemble members. The same ensemble member was also distinguished from the other ensemble members by an El Nino-like mean state anomalies with a steeper background MMG in the SMC region. The abnormal mean state in E10 can be explained by the number of El Nino and La Nina events. In particular, for the 20 years analyzed, E10 experienced La Nina events much less frequently than all other ensemble members.

Examinations of the column water vapor anomalies associated with the MJO revealed that moisture recharging before the onset of MJO convection over SMC and NMC is much greater in E10 than in the other ensemble members. The larger moisture recharging in the two regions is responsible for the stronger MJO propagation across the MC in E10. The column-integrated moisture budget analysis further indicated that the anomalous moisture recharging over the SMC in E10 is primarily associated with the meridional advection of mean moisture by MJO-perturbed wind. The enhanced moistening in the SMC then increases the meridional gradient of intraseasonal moisture to the south of NMC, which was found to be responsible for the enhanced moistening in the NMC.

Our results strongly support the notion that the background moisture gradient in the vicinity of MC plays an important role in the MJO (Gonzalez & Jiang 2017; Jiang 2017). Specifically, the steeper MMG in the SMC is responsible for the larger moisture recharging ahead of MJO convection, resulting in the stronger propagation of the MJO (Ahn et al. 2020b). Our results also demonstrated that changes in the mean state moisture gradient *alone* could lead to substantial changes to MJO propagation characteristics. Ahn et al. (2020a) perturbed a parameter in the cumulus convection scheme only over MC landmasses and examined the associated changes in the mean state and the MJO. They found changes in the mean state and MJO propagation over the oceanic area in the MC where the cumulus convection scheme is not altered, which cannot be attributed to the changes in the interaction between convection and its environment.

The considerable ensemble spread and multi-decadal variability of the background MMG, which is likely to be associated with the ENSO-like internal variability, have implications for low-frequency variability of the MJO activity. Interannual to interdecadal variability of the MJO has been reported both in simulations (Schubert et al., 2013) and in observations (Pohl & Matthews, 2007; Slingo et al., 1999), at least part of which can be explained by the influence of mean state moisture on MJO propagation. Additionally, the assessment of MJO fidelity in the multi-model intercomparison studies might be partly interfered by the internally-varying basic state because most studies use a single ensemble member and a period of equal or less than 20 years (Kim et al., 2009; Hung et al., 2013; Gonzalez & Jiang, 2017; Jiang, 2017; Ling et al., 2017, 2019; Ahn et al., 2017, 2020b). Our results demonstrate the potential added value of evaluating multiple realizations of the same model when available. Future studies of how mean moisture field is modulated by low-frequency climate variability are warranted for further understanding of the interaction between the basic state and the MJO.

There have been attempts to isolate the effects of parameterization changes from that of changes in the mean state (Kelly et al., 2017; Peatman et al., 2018). Using a primitive equation model with no representation of surface turbulent and radiative fluxes, Kelly et al. (2017) constrained the mean state with time-independent forcing and linearized convective heating and moistening processes using the linear response function of Kuang (2010). That way, they could make changes in the convective processes with minimal impacts on the mean state. In a series of aquaplanet simulations, Peatman et al. (2018) examined the effects of moisture entrainment on convectively-coupled equatorial waves with the basic state humidity being constrained. The modeling framework proposed in these studies can potentially be used to study the role of the mean state independent of the effect of parameterization changes, although in both studies constraining the mean state was found to be difficult. Further work is needed to improve the modeling framework that is suitable to study the role of the mean state on tropical waves.

Acknowledgements

This work was funded by the NOAA CVP program (NA18OAR4310300), the DOE RGMA program (DE-SC0016223), the NASA MAP program (80NSSC17K0227), and the KMA R&D program (KMI2018-03110). Work of LLNL-affiliated authors was performed under the auspices of the U.S. Department of Energy by Lawrence Livermore National Laboratory under Contract DE-AC52-07NA27344 and their efforts were supported by the Regional and Global Climate Modeling Program of the United States Department of Energy's Office of Science. We acknowledge the World Climate Research Programme, which, through its Working Group on Coupled Modelling, coordinated and promoted CMIP6. We thank the climate modeling groups for producing and making available their model output, the Earth System Grid Federation (ESGF) for archiving the data and providing access, and the multiple funding agencies who support CMIP6 and ESGF.” We thank DOE’s RGMA program area, the Data Management program, and NERSC for making this coordinated CMIP6 analysis activity possible. The CESM2 Historical simulation data was obtained from the CMIP6 archive (https://esgf-node.llnl.gov/search/cmip6/). The TRMM provided the precipitation data (https://pmm.nasa.gov/data-access/downloads/trmm). The ECMWF provided the fifth generation of ECMWF reanalysis (ERA5, https://www.ecmwf.int/en/forecasts/datasets/reanalysis-datasets/era5).

References

Adames, Á. F., & Kim, D. (2016). The MJO as a dispersive, convectively coupled moisture wave: Theory and observations. *Journal of the Atmospheric Sciences*, *73*(3), 913-941.

Adames, Á. F. (2017). Precipitation budget of the Madden–Julian oscillation. *Journal of the Atmospheric Sciences*, *74*(6), 1799-1817.

Ahn, M.-S., Kim, D., Sperber, K. R., Kang, I.-S., Maloney, E., Waliser, D., & Hendon, H. (2017). MJO simulation in CMIP5 climate models: MJO skill metrics and process-oriented diagnosis. *Climate Dynamics*, *49*(11–12), 4023–4045. https://doi.org/10.1007/s00382-017-3558-4

Ahn, M. S., Kim, D., Park, S., & Ham, Y. G. (2019). Do We Need to Parameterize Mesoscale Convective Organization to Mitigate the MJO-Mean State Trade-Off?. *Geophysical Research Letters*, 46(4), 2293-2301.

Ahn, M. S., Kim, D., Ham, Y. G., & Park, S. (2020a). Role of Maritime Continent Land Convection on the Mean State and MJO Propagation. *Journal of Climate*, *33*(5), 1659-1675.

Ahn, M.-S., Kim, D., Kang, D., Lee, J., Sperber, K. R., Gleckler, P. J., et al. (2020b). MJO propagation across the Maritime Continent: Are CMIP6 models better than CMIP5 models? *Geophysical Research Letters*, *47*, e2020GL087250. https://doi.org/10.1029/2020GL087250

Andersen, J. A., & Kuang, Z. (2012). Moist Static Energy Budget of MJO-like Disturbances in the Atmosphere of a Zonally Symmetric Aquaplanet. *Journal of Climate*, *25*(8), 2782–2804. https://doi.org/10.1175/JCLI-D-11-00168.1

Chikira, M. (2014). Eastward-propagating intraseasonal oscillation represented by Chikira–Sugiyama cumulus parameterization. Part II: Understanding moisture variation under weak temperature gradient balance. *Journal of the Atmospheric Sciences*, *71*(2), 615-639.

Crueger, T., Stevens, B., & Brokopf, R. (2013). The Madden–Julian oscillation in ECHAM6 and the introduction of an objective MJO metric. *Journal of Climate*, *26*(10), 3241-3257.

Danabasoglu, G., Lamarque, J. -F., Bacmeister, J., Bailey, D. A., DuVivier, A. K., Edwards, J., et al. (2020). The Community Earth System Model Version 2 (CESM2). *Journal of Advances in Modeling Earth Systems*, *12*(2), 1–35. https://doi.org/10.1029/2019MS001916

DeMott, C. A., Wolding, B. O., Maloney, E. D., & Randall, D. A. (2018). Atmospheric mechanisms for MJO decay over the Maritime Continent. *Journal of Geophysical Research: Atmospheres*, *123*(10), 5188-5204.

DeMott, C. A., Klingaman, N. P., Tseng, W. L., Burt, M. A., Gao, Y., & Randall, D. A. (2019). The Convection Connection: How Ocean Feedbacks Affect Tropical Mean Moisture and MJO Propagation. *Journal of Geophysical Research: Atmospheres*, *124*(22), 11910–11931. https://doi.org/10.1029/2019JD031015

Eyring, V., Bony, S., Meehl, G. A., Senior, C. A., Stevens, B., Stouffer, R. J., & Taylor, K. E. (2016). Overview of the Coupled Model Intercomparison Project Phase 6 (CMIP6) experimental design and organization. *Geoscientific Model Development*, *9*(5), 1937-1958.

Gonzalez, A. O., & Jiang, X. (2017). Winter mean lower tropospheric moisture over the Maritime

Continent as a climate model diagnostic metric for the propagation of the Madden-Julian oscillation. *Geophysical Research Letters*, *44*(5), 2588–2596. https://doi.org/10.1002/2016GL072430

Hersbach, H., Bell, B., Berrisford, P., Horányi, A., Sabater, J. M., Nicolas, J., et al. (2019). Global reanalysis: Goodbye ERA-Interim, hello ERA5. *ECMWF Newsletter*, *159*, 17–24. https://doi.org/10.21957/vf291hehd7

Holton, J. R., & Hakim, G. J. (2013). *An introduction to dynamic meteorology*. Elsevier.

Huffman, G. J., Bolvin, D. T., Nelkin, E. J., Wolff, D. B., Adler, R. F., Gu, G., et al. (2007). The TRMM Multisatellite Precipitation Analysis (TMPA): Quasi-Global, Multiyear, Combined-Sensor Precipitation Estimates at Fine Scales. *Journal of Hydrometeorology*, *8*(1), 38–55. https://doi.org/10.1175/JHM560.1

Hung, M.-P., Lin, J.-L., Wang, W., Kim, D., Shinoda, T., & Weaver, S. J. (2013). MJO and Convectively Coupled Equatorial Waves Simulated by CMIP5 Climate Models. *Journal of Climate*, *26*(17), 6185–6214. https://doi.org/10.1175/JCLI-D-12-00541.1

Inness, P. M., Slingo, J. M., Woolnough, S. J., Neale, R. B., & Pope, V. D. (2001). Organization of tropical convection in a GCM with varying vertical resolution; implications for the simulation of the Madden-Julian Oscillation. *Climate Dynamics*, *17*(10), 777-793.

Jiang, X. (2017). Key processes for the eastward propagation of the madden-julian oscillation based on multimodel simulations. *Journal of Geophysical Research*, *122*(2), 755–770. https://doi.org/10.1002/2016JD025955

Jones, C., Waliser, D. E., Lau, K. M., & Stern, W. (2004). The Madden–Julian Oscillation and Its Impact on Northern Hemisphere Weather Predictability. *Monthly Weather Review*, *132*(6), 1462–1471. https://doi.org/10.1175/1520-0493(2004)132<1462:TMOAII>2.0.CO;2

Kelly, P., Mapes, B., Hu, I., Song, S., & Kuang, Z. (2017). Tangent linear superparameterization of convection in a 10 layer global atmosphere with calibrated climatology. *Journal of Advances in Modeling Earth Systems*, *9*(2), 932–948. https://doi.org/10.1002/2016MS000871

Kim, D., Sperber, K., Stern, W., Waliser, D., Kang, I.-S., Maloney, E., et al. (2009). Application of MJO Simulation Diagnostics to Climate Models. *Journal of Climate*, *22*(23), 6413–6436. https://doi.org/10.1175/2009JCLI3063.1

Kim, D., Sobel, A. H., Maloney, E. D., Frierson, D. M., & Kang, I. S. (2011). A systematic relationship between intraseasonal variability and mean state bias in AGCM simulations. *Journal of Climate*, *24*(21), 5506-5520.

Kim, Daehyun, Kug, J.-S., & Sobel, A. H. (2014). Propagating versus Nonpropagating Madden–Julian Oscillation Events. *Journal of Climate*, *27*(1), 111–125. https://doi.org/10.1175/JCLI-D-13-00084.1

Kim, D., & Maloney, E. D. (2017). Simulation of the Madden-Julian oscillation using general circulation models. In *The Global Monsoon System: Research and Forecast* (pp. 119-130).

Kuang, Z. (2010). Linear response functions of a cumulus ensemble to temperature and moisture perturbations and implications for the dynamics of convectively coupled waves. *Journal of the Atmospheric Sciences*, *67*(4), 941-962.

Kug, J. S., Jin, F. F., & An, S. I. (2009). Two types of El Niño events: cold tongue El Niño and warm pool

El Niño. *Journal of Climate*, *22*(6), 1499-1515.

Ling, J., Zhang, C., Wang, S., & Li, C. (2017). A new interpretation of the ability of global models to simulate the MJO. *Geophysical Research Letters*, *44*(11), 5798–5806. https://doi.org/10.1002/2017GL073891

Ling, J., Zhao, Y., & Chen, G. (2019). Barrier Effect on MJO Propagation by the Maritime Continent in the MJO Task Force/GEWEX Atmospheric System Study Models. *Journal of Climate*, *32*(17), 5529–5547. https://doi.org/10.1175/jcli-d-18-0870.1

Madden, R. A., & Julian, P. R. (1971). Detection of a 40–50 day oscillation in the zonal wind in the tropical Pacific. *Journal of the Atmospheric Sciences*, *28*(5), 702–708. https://doi.org/10.1175/1520-0469(1971)028<0702:DOADOI>2.0.CO;2

Madden, R. A., & Julian, P. R. (1972). Description of global-scale circulation cells in the tropics with a 40–50 day period. *Journal of the Atmospheric Sciences*, *29*(6), 1109–1123. https://doi.org/10.1175/1520-0469(1972)029<1109:DOGSCC>2.0.CO;2

Maloney, E. D. (2009). The moist static energy budget of a composite tropical intraseasonal oscillation in a climate model. *Journal of Climate*, *22*(3), 711–729. https://doi.org/10.1175/2008JCLI2542.1

Mapes, B., & Neale, R. (2011). Parameterizing convective organization to escape the entrainment dilemma. *Journal of Advances in Modeling Earth Systems*, *3*(2).

Neena, J. M., Lee, J. Y., Waliser, D., Wang, B., & Jiang, X. (2014). Predictability of the Madden–Julian Oscillation in the Intraseasonal Variability Hindcast Experiment (ISVHE). *Journal of Climate*, *27*(12), 4531–4543. https://doi.org/10.1175/JCLI-D-13-00624.1

Peatman, S. C., Matthews, A. J., & Stevens, D. P. (2014). Propagation of the Madden-Julian Oscillation through the Maritime Continent and scale interaction with the diurnal cycle of precipitation. *Quarterly Journal of the Royal Meteorological Society*, *140*(680), 814–825. https://doi.org/10.1002/qj.2161

Peatman, S. C., Methven, J., & Woolnough, S. J. (2018). Isolating the effects of moisture entrainment on convectively coupled equatorial waves in an aquaplanet GCM. *Journal of the Atmospheric Sciences*, *75*(9), 3139–3157. https://doi.org/10.1175/JAS-D-18-0098.1

Pohl, B., & Matthews, A. J. (2007). Observed Changes in the Lifetime and Amplitude of the Madden–Julian Oscillation Associated with Interannual ENSO Sea Surface Temperature Anomalies. *Journal of Climate*, *20*(11), 2659–2674. https://doi.org/10.1175/JCLI4230.1

Raymond, D. J., & Fuchs, Ž. (2009). Moisture modes and the Madden–Julian oscillation. *Journal of Climate*, *22*(11), 3031-3046.

Rayner, N. A. A., Parker, D. E., Horton, E. B., Folland, C. K., Alexander, L. V., Rowell, D. P., ... & Kaplan, A. (2003). Global analyses of sea surface temperature, sea ice, and night marine air temperature since the late nineteenth century. *Journal of Geophysical Research: Atmospheres*, *108*(D14).

Schubert, J. J., Stevens, B., & Crueger, T. (2013). Madden-Julian oscillation as simulated by the MPI Earth System Model: Over the last and into the next millennium. *Journal of Advances in Modeling Earth Systems*, *5*(1), 71–84. https://doi.org/10.1029/2012MS000180

Sobel, A., & Maloney, E. (2012). An idealized semi-empirical framework for modeling the Madden–Julian oscillation. *Journal of the Atmospheric Sciences*, *69*(5), 1691-1705.

Sobel, A., & Maloney, E. (2013). Moisture modes and the eastward propagation of the MJO. *Journal of the Atmospheric Sciences*, *70*(1), 187-192.

Slingo, J. M., Sperber, K. R., Boyle, J. S., Ceron, J. P., Dix, M., Dugas, B., et al. (1996). Intraseasonal oscillations in 15 atmospheric general circulation models: Results from an AMIP diagnostic subproject. *Climate Dynamics*, *12*(5), 325-357.

Slingo, J. M., Rowell, D. P., Sperber, K., & Nortley, F. (1999). On the predictability of the interannual behaviour of the Madden-Julian Oscillation and its relationship with El Niño. *Quarterly Journal of the Royal Meteorological Society*, *125*(554), 583–609. https://doi.org/10.1256/smsqj.55410

Zhang, C. (2013). Madden-julian oscillation: Bridging weather and climate. *Bulletin of the American Meteorological Society*, *94*(12), 1849–1870. https://doi.org/10.1175/BAMS-D-12-00026.1

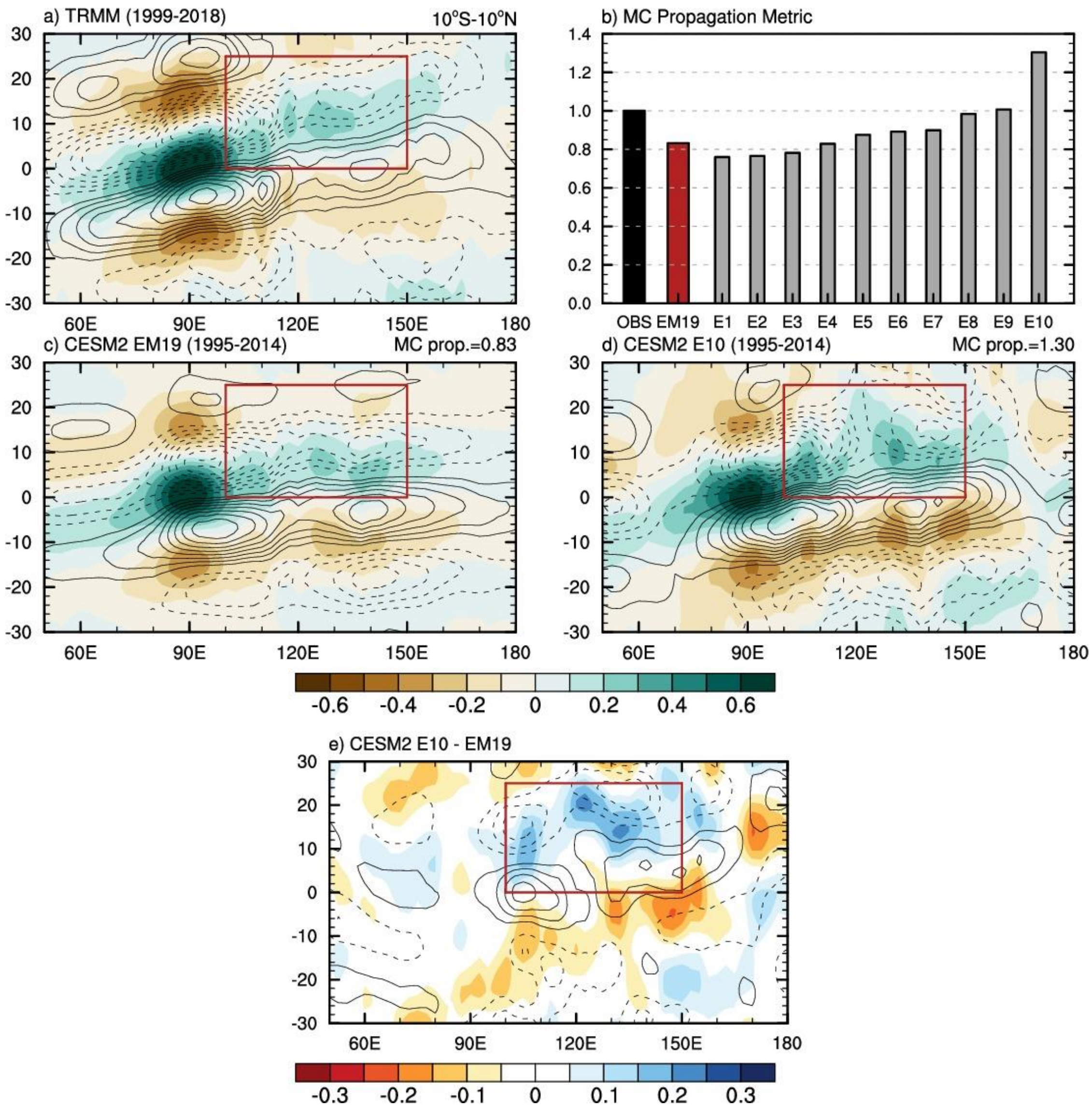

Figure 1. (a) Longitude-time evolution of 20-100 day bandpass-filtered TRMM precipitation (shaded; the unit is mm day^{-1}) and ERA5 column-integrated moisture tendency (contour; kg m^{-2} s^{-1}) near the equator (10°S–10°N) regressed onto the precipitation averaged in the IO base point (85–95°E, 5°S–5°N) for 1999-2018. (b) The MC propagation metric of TRMM, the ensemble mean through E1 to E9 (EM19), and each ensemble member in ascending order. (c-d) Same as (a), but for (c) the EM19 and (d) the E10 of CESM2 for 1995-2014. (e) Difference between E10 and EM19. The red boxes indicate a domain for the MC propagation metric.

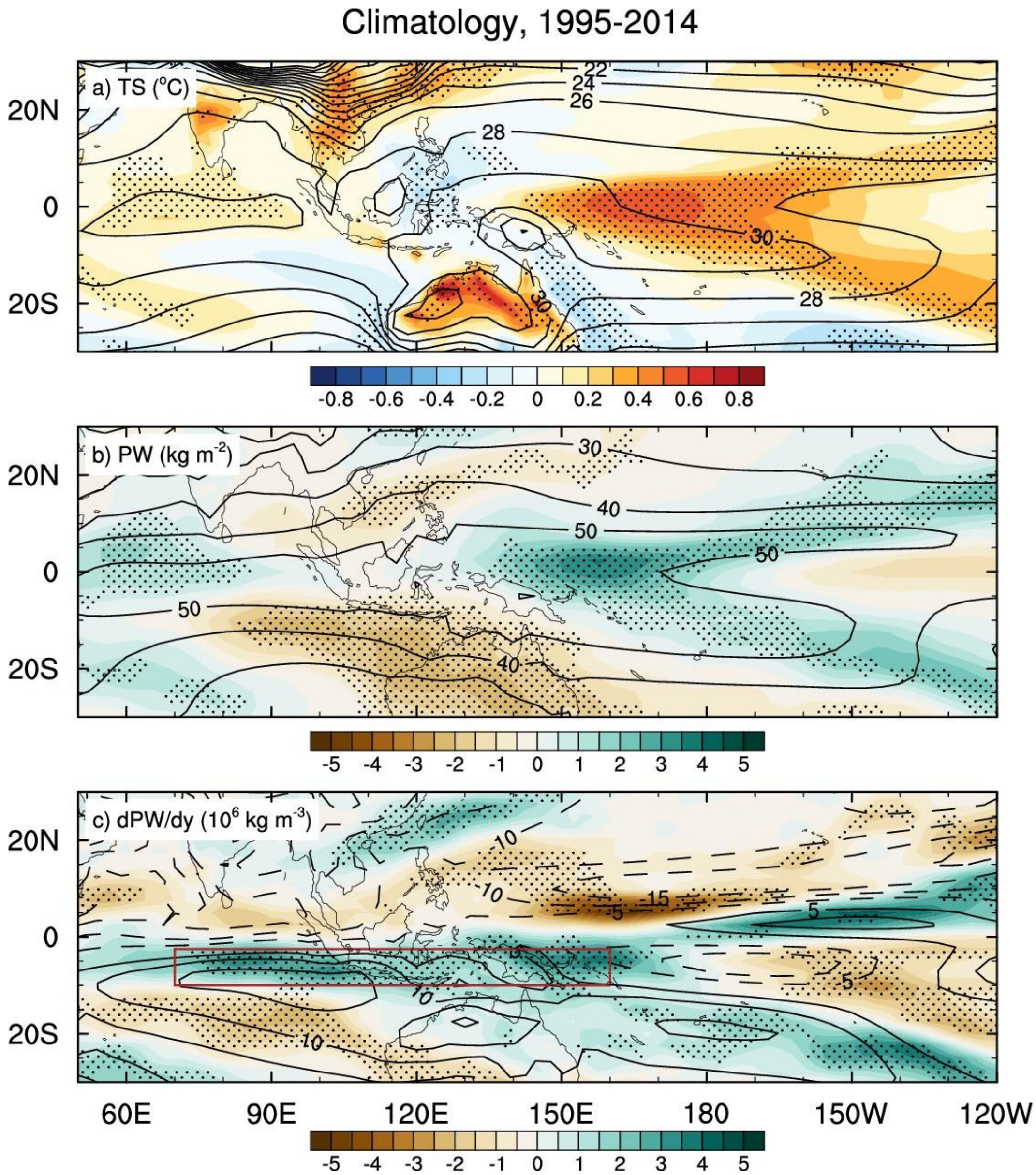

Figure 2. Climatology during boreal winter for 1995-2014 in the EM19 (contour) and the difference between E10 and EM19 (shaded). Each panel shows (a) surface temperature (°C), (b) precipitable water (kg m^{-2}), and (c) meridional gradient of precipitable water (10^6 kg m^{-3}). Areas with black dots indicate the E10 higher (lower) than the maximum (minimum) value of the nine ensembles involved in the EM19.

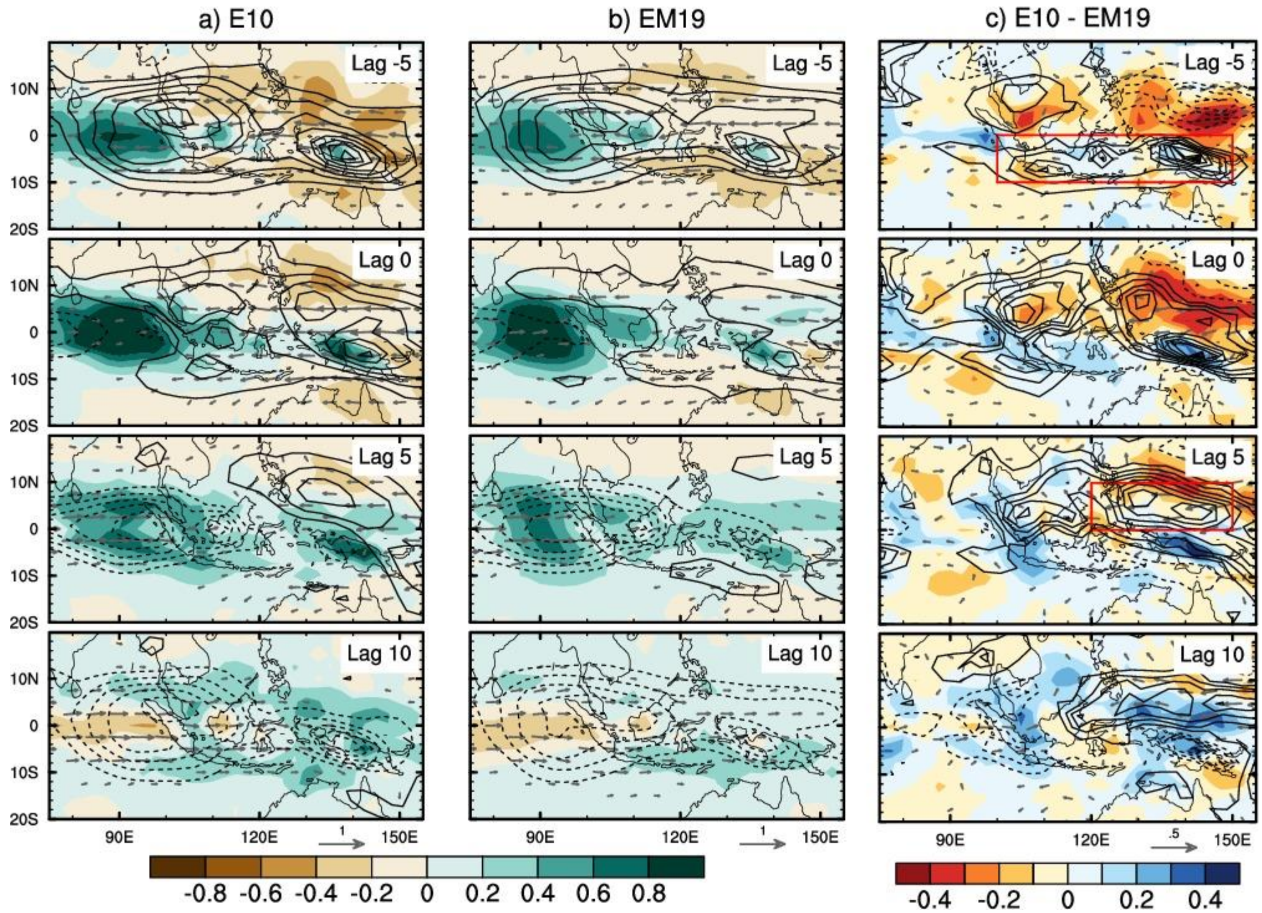

Figure 3. Lagged regression of 20-100 day bandpass-filtered precipitation (shaded; mm day^{-1}), column-integrated moisture tendency (contour; kg m^{-2} s^{-1}), and horizontal wind at 850 hPa (vector; m s^{-1}) regressed onto the precipitation averaged in the IO base point (85–95°E, 5°S–5°N). Each panel refers (a) the E10, (b) the EM19, and (c) difference between the E10 and the EM19. The red boxes on lag -5 and 5 in Figure 3c indicate the SMC and the NMC, respectively.

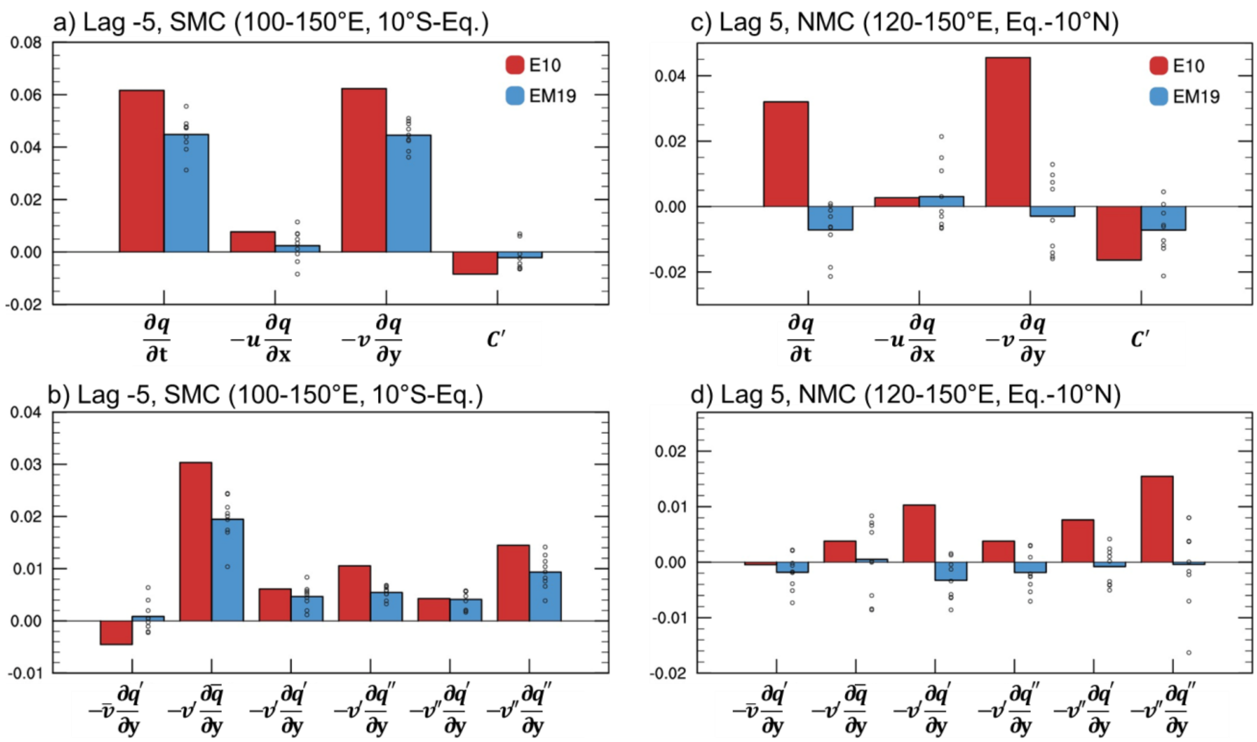

Figure 4. (a) Moisture budget terms averaged in the southern MC (100–150°E, 10°S–Eq.; the red box at lag -5 in Figure 3c; kg m^{-2} s^{-1}) regressed onto intraseasonal precipitation (mm day^{-1}) in the IO base point. (b) Timescale decompositions of the moisture gradient and meridional wind terms. The timescale decomposition terms of very small values are not shown. (c-d) Same as (a-b), but in the NMC at lag 5 (120–150°E, Eq.–10°N; the red box at lag 5 in Figure 3c). All terms shown in the bar graphs are column-integrated, 20–100 day bandpass-filtered, and spatially weighted by the convective moisture adjustment frequency.